

# Lithium Titanate Anode Thin Films for Li-Ion Solid State Battery Based on Garnets

Reto Pfenninger,\* Semih Afyon, Iñigo Garbayo, Michal Struzik, and Jennifer L. M. Rupp

Solid state electrolytes, such as Li-Garnets, are fastest Li-ionic conductor materials that have attracted attention for safe hybrid and full solid state battery architectures. Turning to oxide-based low voltage anodes gives opportunities to avoid Li-dendrite formation and also to reach full thin film microbattery architectures based on garnets as high energy density replacement for supercapacitors. Herein, it is demonstrated that  $\text{Li}_4\text{Ti}_5\text{O}_{12}$  thin films deposited by pulsed laser deposition can show stable structures and cycling kinetics reaching almost close to theoretical capacity of  $175 \text{ mAh g}^{-1}$  when combined to  $\text{Li}_{6.25}\text{Al}_{0.25}\text{La}_3\text{Zr}_2\text{O}_{12}$  pellets. Stable operation at room temperature with 90% of theoretical capacity retention at  $2.5 \text{ mA g}^{-1}$  over 22 cycles is achieved on bilayer half cell batteries. Rate capability studies show promising charge and discharge capacities and act as a case study for the well-known  $\text{Li}_4\text{Ti}_5\text{O}_{12}$  thin film anode, demonstrating its good compatibility with the investigated solid garnet electrolyte. This gives new perspective on the use of oxide-based low voltage anodes for future strategies avoiding Li-dendrite formation or safe solid state microbattery thin film assemblies based on Li-garnets.

maintaining the device material structures are also equally important.<sup>[2]</sup> Here, all-solid-state batteries are promising, since they show superior chemical stability, better packaging<sup>[3,4]</sup> and improved safety (i.e., no inflammable liquids<sup>[5]</sup>). In addition, one may even use the opportunity to gain higher endurance during operation and option to work at high temperatures to further enhance its Li diffusion kinetics. Latter is attractive if we consider integrating solid state battery components as future integrated circuit components co-operating and managing waste heat for chip architectures<sup>[6]</sup> in the internet of things or simply for industrial large-scale power management.

Considering the scalability, ceramic all-solid-state battery constituents are easily transferrable to thin film microbattery architectures<sup>[7,8]</sup> for powering of portable electronics and chip units such as sensors or actuators. Recent reports show clear potential to surge

## 1. Introduction

Next generation energy storage technologies for stationary and mobile electronics rely on materials and devices with high gravimetric and volumetric capacity.<sup>[1]</sup> Safety aspects such as operation in rough environments and at a widened temperature window

forward to replace supercapacitor structures.<sup>[9]</sup> This is on the one hand due to the high inherent energy densities of solid microbatteries, which can omit by their nature classic packaging requirements and also minimize electrode distances by the employment of thin film processing of the components by two to three orders of magnitude.<sup>[10–12]</sup> Comparing state-of-the-art performances, up to  $7.4 \text{ mW cm}^{-2} \mu\text{m}^{-1}$  can currently be reached as recently demonstrated by Lewis group for a NiSn/LiMnO<sub>2</sub>-based hybrid microbattery showing high potential, but still including a liquid type electrolyte.<sup>[7,9]</sup> Now, using solid state thin film techniques classic liquid and polymer separators can be eliminated for a simplified structure, whereby high packaging density and safety are improved and Li diffusion length is shortened due to its tenth of nanometer in film thickness, as demonstrated by the Van Notten group.<sup>[3]</sup>

Looking at feasible all-solid state electrolytes, it becomes apparent that several requirements on such materials are desired, among which high lithium ionic conductivity, the temperature and mechanical stability, and chemical stability versus metallic lithium are equally important. Among the different all-solid state electrolytes available today<sup>[13]</sup> (e.g., Na Super Ionic CONductor,<sup>[14–16]</sup> Li Super Ionic CONductor,<sup>[17–19]</sup> or Li Phosphorous Oxy-Nitride<sup>[20]</sup>) cubic garnet  $\text{Li}_7\text{La}_3\text{Zr}_2\text{O}_{12}$  (LLZO)-based structures<sup>[21]</sup> are of particular interest. First reported by Weppner and co-workers,<sup>[22]</sup> LLZO with fast Li<sup>+</sup>-conduction of up to  $1 \text{ mS cm}^{-1}$  has been demonstrated at room

R. Pfenninger, Dr. S. Afyon, Dr. I. Garbayo, Dr. M. Struzik,  
Prof. J. L. M. Rupp  
Electrochemical Materials  
Department of Material Science  
ETH Zurich, 8049 Zürich, Switzerland  
E-mail: reto.pfenninger@mat.ethz.ch

R. Pfenninger, Dr. M. Struzik, Prof. J. L. M. Rupp  
Electrochemical Materials  
Department of Material Science and Engineering  
Massachusetts Institute of Technology  
77 Massachusetts Ave, Cambridge, MA 02139, USA

Prof. J. L. M. Rupp  
Electrochemical Materials  
Department of Electrical Engineering and Computer Science  
Massachusetts Institute of Technology  
77 Massachusetts Ave, Cambridge, MA 02139, USA

 The ORCID identification number(s) for the author(s) of this article can be found under <https://doi.org/10.1002/adfm.201800879>.

DOI: 10.1002/adfm.201800879

temperature<sup>[21]</sup> that positions the garnets as one of the highest solid-state inorganic Li<sup>+</sup> conductors available. Li<sub>7</sub>La<sub>3</sub>Zr<sub>2</sub>O<sub>12</sub> exhibits two different crystallographic phases, a low conductive tetragonal phase and a high conductive cubic phase, as first described by Awaka et al.<sup>[23,24]</sup> However, the stabilization of the cubic Li<sub>7</sub>La<sub>3</sub>Zr<sub>2</sub>O<sub>12</sub> phase at room temperature is challenging, as is its processing to dense ceramic pellets due to Li-losses at elevated temperatures.<sup>[25,26]</sup> Different attempts to stabilize these structures by doping on either the Li-site (Ga<sup>3+</sup> and Al<sup>3+</sup>),<sup>[25,27–29]</sup> the La-site (Nd<sup>3+</sup>, Sr<sup>2+</sup>),<sup>[22,30,31]</sup> or the Zr-site (mainly Ta<sup>5+</sup>)<sup>[32,33]</sup> have been successful. Among the highest Li conductivities and stable structures have been achieved through, doping on the Li-site with Al<sup>3+</sup>,<sup>[34–36]</sup> which we will depict through this study as the solid state electrolyte material of choice. Furthermore, transferability to thin film form has been shown to be challenging and is not yet fully understood, leaving a lot of room for improvement to the field, thus giving reasons to the importance of understanding electrode interactions and battery performance starting from bulk pellet-based model systems first.

From an electrode perspective, all-solid-state batteries have the potential to integrate new and mostly unexplored high capacity and energy electrode materials such as vanadate-based<sup>[37]</sup> or sulfur<sup>[38]</sup>-based composites which show conventionally a low stability in standard liquid or polymer-based Li-ion batteries for long term cycling. Despite the progress on LLZO as a solid state electrolyte, only a few systematic studies have been conducted on the combination of electrodes with garnet-type Li<sub>7</sub>La<sub>3</sub>Zr<sub>2</sub>O<sub>12</sub> electrolytes, so far; viz. the chemical stability and operation conditions of full LLZO-based battery cells are still under discussion.<sup>[39]</sup> Previously, main focus in the field has been set on pulsed laser deposition (PLD) and investigation of *cathodes* for Li-garnet electrolytes: i.e., LiCoO<sub>2</sub> cathodes, see Asaoka group, reporting capacities of 130 mAh g<sup>-1</sup> with cycling stability challenges.<sup>[40–43]</sup> Very recently, first oxide-based *anodes* of Li<sub>4</sub>Ti<sub>5</sub>O<sub>12</sub> were fused with Li-garnets and successfully cycled as stable solid state batteries based on cost-effective ceramic processing by Van den Broek et al.<sup>[44]</sup> Apart from this, there is only one additional literature report on Al-doped Li<sub>7</sub>La<sub>3</sub>Zr<sub>2</sub>O<sub>12</sub> electrolyte in a battery assembly with Li<sub>4</sub>Ti<sub>5</sub>O<sub>12</sub> and LiMn<sub>2</sub>O<sub>4</sub> by Jin and Mc Ginn.<sup>[45]</sup> In general, the anode material Li<sub>4</sub>Ti<sub>5</sub>O<sub>12</sub> crystallizes with space group *Fd-3m* and was shown to be a mechanically very stable battery-anode material for tests upon standard liquid electrolytes. With 175 mAh g<sup>-1</sup> theoretical capacity,<sup>[46]</sup> Li<sub>4</sub>Ti<sub>5</sub>O<sub>12</sub> remains moderate with an average voltage of ≈1.5 V versus Li when tested in liquid electrolyte-based Li-ion batteries.<sup>[47]</sup> However, fast discharge rates,<sup>[48]</sup> a flat voltage profile<sup>[49]</sup> at around 1.5 V and very similar lattice parameters of the fully delithiated phase Li<sub>4</sub>Ti<sub>5</sub>O<sub>12</sub> and the lithiated phase Li<sub>7</sub>Ti<sub>5</sub>O<sub>12</sub> give rise to very low lattice strain upon cycling which is attractive to manage the chemomechanics.<sup>[50]</sup> The latter is particularly important in the case of all-solid-state batteries, since induced strain due to large volume expansion during lithiation/delithiation is one of the main causes of cracks, delamination and poor battery performances potentially restricting lifetime for all-solid batteries. Here ceramic processing strategies to form strong interfacial bonds between the electrolyte and the electrode are needed, as is the electrochemical study of the material interface Li<sub>4</sub>Ti<sub>5</sub>O<sub>12</sub> anode/Li<sub>7</sub>La<sub>3</sub>Zr<sub>2</sub>O<sub>12</sub> electrolyte. One challenge that needs to be addressed particularly for future microbattery integration

of Li-garnets is the processing of Li<sub>4</sub>Ti<sub>5</sub>O<sub>12</sub> in the form of thin films. In this regard, several attempts have also been taken already to deposit Li<sub>4</sub>Ti<sub>5</sub>O<sub>12</sub> as thin films either by radio frequency-sputtering,<sup>[51]</sup> sol-gel method<sup>[52]</sup> or PLD<sup>[53–55]</sup> on classic Li-electrolytes such as quartz, oriented Al<sub>2</sub>O<sub>3</sub>, MgAl<sub>2</sub>O<sub>4</sub>, or coated silicon substrates. Testing in liquid-based electrolytes have usually shown capacities around 90% of the theoretical maximum.<sup>[53]</sup> It remains open at this point whether nanograined Li<sub>4</sub>Ti<sub>5</sub>O<sub>12</sub> films are electrochemically stable toward Li-garnets in terms of their interface. Recent progress of Van den Broek et al.<sup>[44]</sup> does confirm high stability for micrometer-sized thicknesses of ≈40–50 μm slurry-coated layers when combined with Li-garnet bulk pellets. However, at the thin film level, the nanoscopic grain structures and high grain boundary volumes may lead to differed Li-ionic transfer and capacities,<sup>[56,57]</sup> which are to be explored, in particular in very low C-rate cycling with careful focus on the observable oxidation and reduction reactions. Besides, it is known that strain effects can strongly be imposed when turning to thin film, which can alter even the interfacial impedance characteristics toward a solid electrolyte and can vary the ionic transfer over orders of magnitude.<sup>[58,59]</sup> Despite the effort of the transfer, all-solid-batteries of Li-garnet structures with thin films of the anode material Li<sub>4</sub>Ti<sub>5</sub>O<sub>12</sub> still have to be constructed and tested thoroughly. It remains even unclear from previous reports, whether such interfaces of pellet-Li<sub>7</sub>La<sub>3</sub>Zr<sub>2</sub>O<sub>12</sub>/anode-Li<sub>4</sub>Ti<sub>5</sub>O<sub>12</sub> electrode are stable, for which thin film structures are viable objects of study. The implication of these investigations would further allow to judge on the potential of Li<sub>4</sub>Ti<sub>5</sub>O<sub>12</sub> material as an alternative to pure Li anodes in safe and large scale ceramic batteries with extended temperature window but also as thin-film anode material for future microbattery architectures. In addition, we rate the exploration of alternative anodes for Li-garnet solid state electrolytes as significant as also recent reports of Aguesse et al.<sup>[60]</sup> revealed that the employment of pure lithium may lead to short circuiting by Li dendritic growth upon prolonged cycling. From a general materials perspective, one may learn deeply from the anode-application use of Li<sub>4</sub>Ti<sub>5</sub>O<sub>12</sub> as it has been studied extensively in the field of liquid electrolyte-based batteries<sup>[49,61–63]</sup> and hybrid cell microbattery applications,<sup>[7]</sup> for example, where Li<sub>4</sub>Ti<sub>5</sub>O<sub>12</sub> has been 3D printed on a glassy substrate immersed in a liquid electrolyte. In essence, we see a huge prospect for integration and novel battery cells combining the Li<sub>4</sub>Ti<sub>5</sub>O<sub>12</sub> in the form of thin films to Li-garnets as model structures to understand the interface stability and electrochemistry for large-scale battery storage and particularly in the area of thin film microbatteries.

Through this work, we demonstrate the fabrication and investigate all-solid-state Li-ion batteries combining the anode material Li<sub>4</sub>Ti<sub>5</sub>O<sub>12</sub> in the form of thin films with the Li-garnet electrolyte c-Li<sub>6,25</sub>Al<sub>0,25</sub>La<sub>3</sub>Zr<sub>2</sub>O<sub>12</sub>. We show composition control and deposition of dense and crack-free Li<sub>4</sub>Ti<sub>5</sub>O<sub>12</sub> thin films on Li-garnet pellets as well as on single crystalline substrates such as MgO. We probe the near order vibrational characteristics and confirm their phase stability when deposited as thin films via Raman spectroscopy. Electrochemical impedance spectroscopic techniques were employed to investigate the impedances relative to the nanostructure and phase for the anode thin films of Li<sub>4</sub>Ti<sub>5</sub>O<sub>12</sub>. Eventually, we probe the lithium dynamics in charging and discharging, as well as its incorporation to Li<sub>4</sub>Ti<sub>5</sub>O<sub>12</sub> electrodes

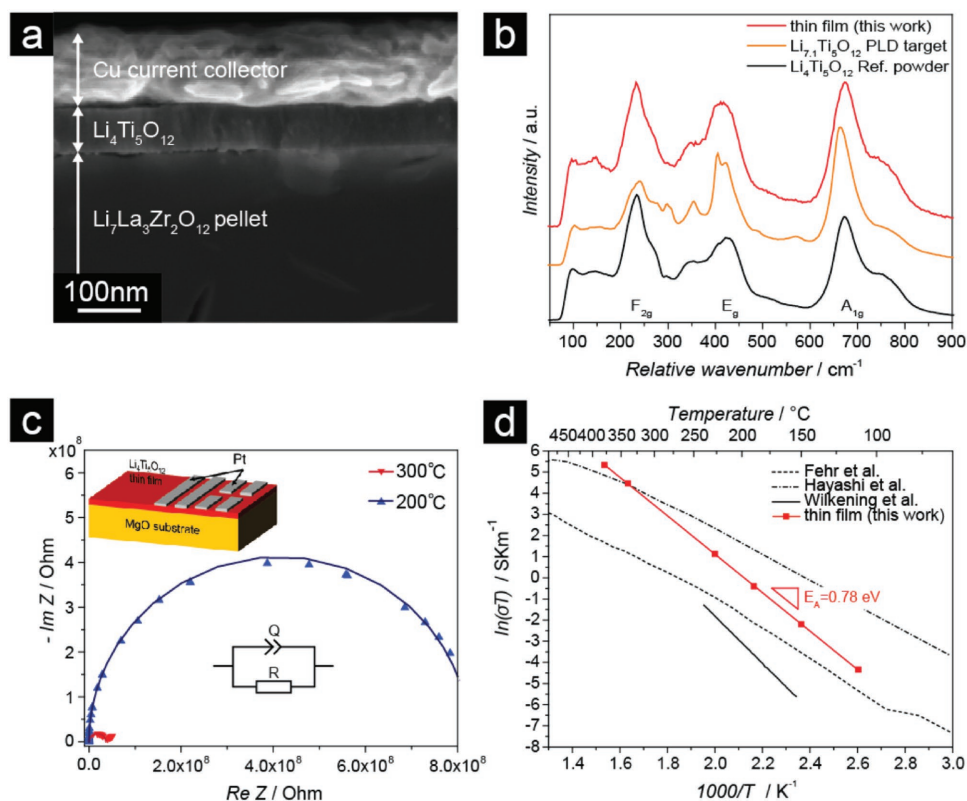


**Figure 1.** a) Cross-sectional SEM image of a  $\text{Li}_4\text{Ti}_5\text{O}_{12}$  thin film deposited by pulsed laser deposition on an electrolyte substrate. b) Raman spectra of thin film of  $\text{Li}_4\text{Ti}_5\text{O}_{12}$  deposited on MgO recorded with 10 mW power and 532 nm wavelength and comparison to powder reference patterns ( $\text{Li}_4\text{Ti}_5\text{O}_{12}$ ) as well as overlithiated PLD target ( $\text{Li}_{7.1}\text{Ti}_5\text{O}_{12}$ ). c) Nyquist plot of impedance measured in in-plane geometry with platinum top contacts at 200 and 300 °C, respectively (dots) and fitting according to a resistive element in parallel with a constant-phase-element (lines). d) Arrhenius plot of  $\text{Li}_4\text{Ti}_5\text{O}_{12}$  thin film on MgO. The thin film is compared toward literature references obtained from  $\text{Li}_4\text{Ti}_5\text{O}_{12}$  pellets. The activation energy of 0.78 eV is in line with pellet dc-conductivity as well as spin-alignment echo (SAE) nuclear magnetic resonance (NMR) spectroscopy reported in literature.<sup>[67,68,79]</sup>

in combination with the Li-garnet electrolyte, studying the development of cell potential and capacity with respect to (dis)charge rates toward Li counter electrode. Ultimately, we conclude on the potential of lithium titanate anodes as future electrodes for Li-garnet electrolytes, discuss their stability as solid-solid interfaces for large scale storage and microbattery applications.

## 2. Results and Discussion

### 2.1. Thin Films of $\text{Li}_4\text{Ti}_5\text{O}_{12}$ Anodes on MgO Substrates

We first turn to the investigation of the anode  $\text{Li}_4\text{Ti}_5\text{O}_{12}$  thin film microstructure and its crystallinity after PLD deposition on MgO substrates. **Figure 1a** displays the cross-sectional SEM image of a thin film deposition of lithium titanate of roughly  $80 \pm 5 \text{ nm}$  in thickness deposited on an electrolyte pellet. A continuous, flat, and dense microstructure was observed for the  $\text{Li}_4\text{Ti}_5\text{O}_{12}$  anode films forming a sharp interface after deposition toward the  $\text{Li}_{6.25}\text{Al}_{0.25}\text{La}_3\text{Zr}_2\text{O}_{12}$  pellet electrolyte. (Lower magnification SEM images of the electrolyte pellet as well as the thin film grown on the electrolyte can be found in Figure S4a,b, Supporting Information, respectively). Microstructure of the  $\text{Li}_4\text{Ti}_5\text{O}_{12}$  films reveals tendency of slightly columnar grain growth. We use Raman spectroscopy as well as XRD (Figure S1,

Supporting Information) to analyze the phase constituents of the  $\text{Li}_4\text{Ti}_5\text{O}_{12}$  film (Figure 1b). Herein, Raman spectrum of the thin film is compared versus the respective powder reference data for  $\text{Li}_4\text{Ti}_5\text{O}_{12}$  powder and to the overlithiated  $\text{Li}_{7.1}\text{Ti}_5\text{O}_{12}$  PLD target in use. In general, three main Raman active bands can be observed for pure  $\text{Li}_4\text{Ti}_5\text{O}_{12}$  positioned at 671, 421, and 231  $\text{cm}^{-1}$  corresponding to the symmetric stretching vibration mode  $\text{A}_{1g}$  of the Ti–O bond, the asymmetric stretching mode  $\text{E}_g$  of the Li–O bond and the bending vibration mode  $\text{F}_{2g}$  of the Ti–O, respectively. These are well distinguished in the deposited lithium titanate films, whose spectra match perfectly with the reference powder, thus confirming the formation of the spinel  $\text{Li}_4\text{Ti}_5\text{O}_{12}$  in the films as deposited from the overlithiated  $\text{Li}_{7.1}\text{Ti}_5\text{O}_{12}$  target. We also note additional Raman vibrations at  $\approx 300 \text{ cm}^{-1}$  and peak splitting are around 421  $\text{cm}^{-1}$  which are ascribed to Li-vibrations occurring from the strong overlithiation for the pellet target, this is in line with previous pellet-based reports from literature.<sup>[64–66]</sup>

To study the implication on the Li-transfer of the deposited film to the MgO substrate, we now turn to electrochemical impedance spectroscopy probing the Li-ionic transport kinetics. Figure 1c shows an example of two impedance spectra acquired in the deposited films with zero bias at two selected measuring temperatures, being 200 and 300 °C. The in-plane measuring configuration with top rectangular platinum electrodes is depicted as an inset of Figure 1c. Analyzing the Nyquist plot, we

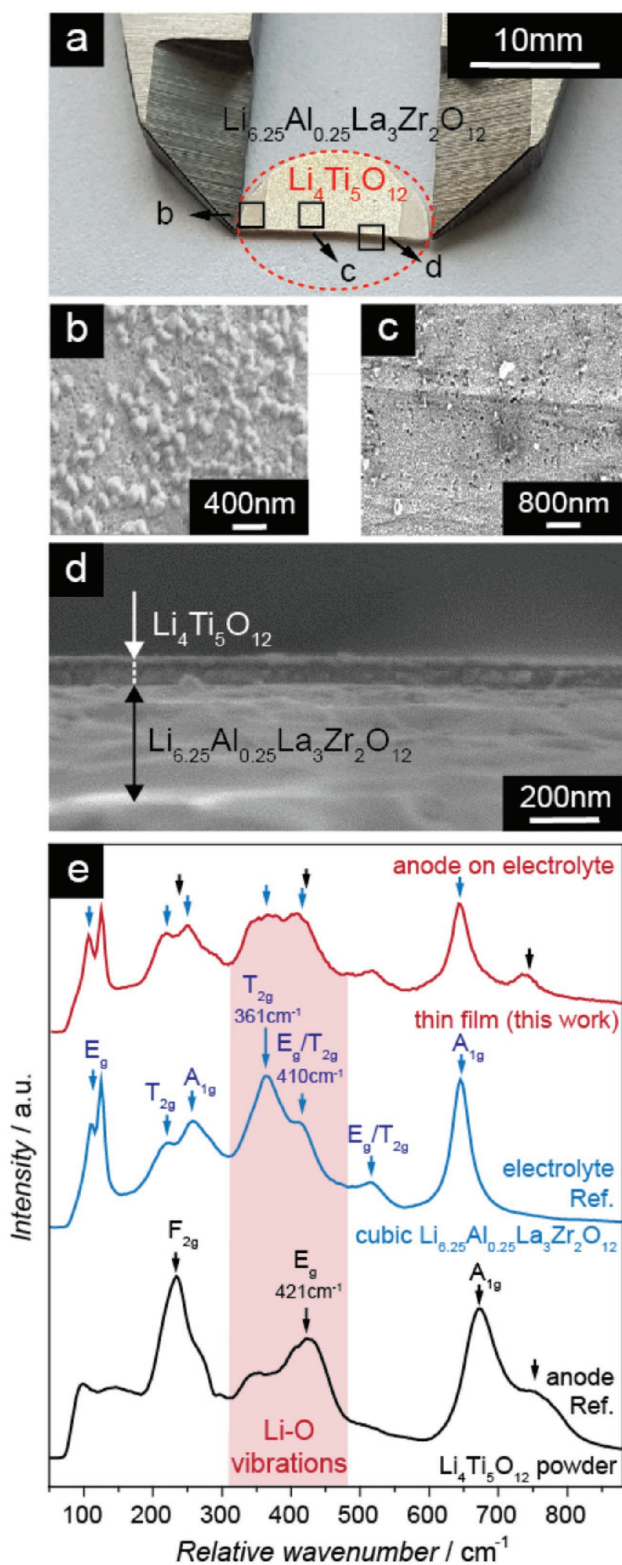


**Figure 2.** a) Optical image of  $\text{Li}_{6.25}\text{Al}_{0.25}\text{La}_3\text{Zr}_2\text{O}_{12}$  pellet with thin film of  $\text{Li}_4\text{Ti}_5\text{O}_{12}$  on top. b, c) SEM images of the surface morphologies at different magnifications. d) Cross-sectional SEM image of the  $\text{Li}_{6.25}\text{Al}_{0.25}\text{La}_3\text{Zr}_2\text{O}_{12}/\text{Li}_4\text{Ti}_5\text{O}_{12}$  heterostructure. e) Raman spectra recorded with 10 mW power and 532 nm wavelength of the respective thin film/target and comparison to powder reference patterns recorded in our lab ( $\text{Li}_4\text{Ti}_5\text{O}_{12}$ ).

confirm a clear semicircle for the impedance at high frequencies with an additional tail attributed to the platinum blocking electrodes (see Figure S2, Supporting Information) based on frequency comparison and literature. Impedance characteristics of the system shown in this geometry contain contributions from both majority ionic as well as potential minority electronic transport. The first semicircle was therefore attributed to the thin film and fitted to an equivalent circuit model of a resistor in parallel with a constant-phase element. We employ the resistance fitted by the equivalent circuit model for the  $\text{Li}_4\text{Ti}_5\text{O}_{12}$  thin film to study the Arrhenius behavior of conductivity. In Figure 1d, the thin film of  $\text{Li}_4\text{Ti}_5\text{O}_{12}$  grown on (001) MgO is compared to literature of spinel  $\text{Li}_4\text{Ti}_5\text{O}_{12}$  bulk pellet.<sup>[67,68]</sup> Both, the measured activation energy of 0.78 eV and the calculated conductivity are in agreement with values obtained in literature for  $\text{Li}_4\text{Ti}_5\text{O}_{12}$  pellets such as of Wilkening et al., which also shows some spread.<sup>[67,68]</sup> We find a one to two orders of magnitude lowered conductivity measured for the nanocrystalline  $\text{Li}_4\text{Ti}_5\text{O}_{12}$  thin films, when compared to the macrocrystalline bulk pellets. However, it is important to highlight here that transfer from microcrystalline pellets to nanocrystalline thin film often lowers conductivity due to the changed grain-to-grain boundary volume ratio, see, i.e., ref. [69]. This is also a known phenomenon in other classes of oxides.<sup>[70–72]</sup>

Based on the results obtained from this thin film processing and structural analysis we confirm for  $\text{Li}_4\text{Ti}_5\text{O}_{12}$  on MgO that dense  $\text{Li}_4\text{Ti}_5\text{O}_{12}$  thin films can be deposited in the desired phase of spinel  $\text{Li}_4\text{Ti}_5\text{O}_{12}$  and can now be grown on  $\text{Li}_{6.25}\text{Al}_{0.25}\text{La}_3\text{Zr}_2\text{O}_{12}$  electrolyte ceramic pellets to be investigated as all-solid-state battery assembly in the following.

## 2.2. Thin Films of $\text{Li}_4\text{Ti}_5\text{O}_{12}$ on Li-Garnet $\text{Li}_{6.25}\text{Al}_{0.25}\text{La}_3\text{Zr}_2\text{O}_{12}$ Substrates for Pellet-Based Battery Assemblies

We now turn to the battery assembly for which  $\text{Li}_4\text{Ti}_5\text{O}_{12}$  films were grown by PLD on home-made dense  $\text{Li}_{6.25}\text{Al}_{0.25}\text{La}_3\text{Zr}_2\text{O}_{12}$  pellets. The microstructure of  $\text{Li}_4\text{Ti}_5\text{O}_{12}$  films deposited on the electrolyte pellets (Figure 2a), which was investigated by SEM and is displayed in Figure 2b–d. The top view of the polished electrolyte pellet surface with PLD-deposited  $\text{Li}_4\text{Ti}_5\text{O}_{12}$  thin film on top exhibits homogeneously flat and continuous microstructure for the thin film anode (Figure 2c), opposed to that of a fresh polished pellet surface without thin film (Figure 2b). It is assumed that the particle agglomerates in that image formed during exposure of the pellet to ambient atmosphere. Since  $\text{Li}_7\text{La}_3\text{Zr}_2\text{O}_{12}$  is known for reacting with humidity and  $\text{CO}_2$ , to form  $\text{Li}_2\text{CO}_3$ <sup>[73,74]</sup> on the surface of the pellet without  $\text{Li}_4\text{Ti}_5\text{O}_{12}$  coating, as observed also by other investigators.<sup>[27]</sup> In Figure 2d, cross-sectional SEM has been performed on the anode film/electrolyte pellet interface before battery cycling.

In Figure 2e, the Raman spectra of the battery half-cell comprised of  $\text{Li}_4\text{Ti}_5\text{O}_{12}$  thin film deposited on the  $\text{Li}_{6.25}\text{Al}_{0.25}\text{La}_3\text{Zr}_2\text{O}_{12}$  pellet is displayed and compared to an anode powder of  $\text{Li}_4\text{Ti}_5\text{O}_{12}$  and an electrolyte  $\text{Li}_{6.25}\text{Al}_{0.25}\text{La}_3\text{Zr}_2\text{O}_{12}$ . Here, the observed spectrum shows bands from thin film of  $\text{Li}_4\text{Ti}_5\text{O}_{12}$  as well as contribution from the underlying electrolyte substrate. This is expected, since the penetration depth of the Raman signal were to penetrate more than the 80 nm of thin

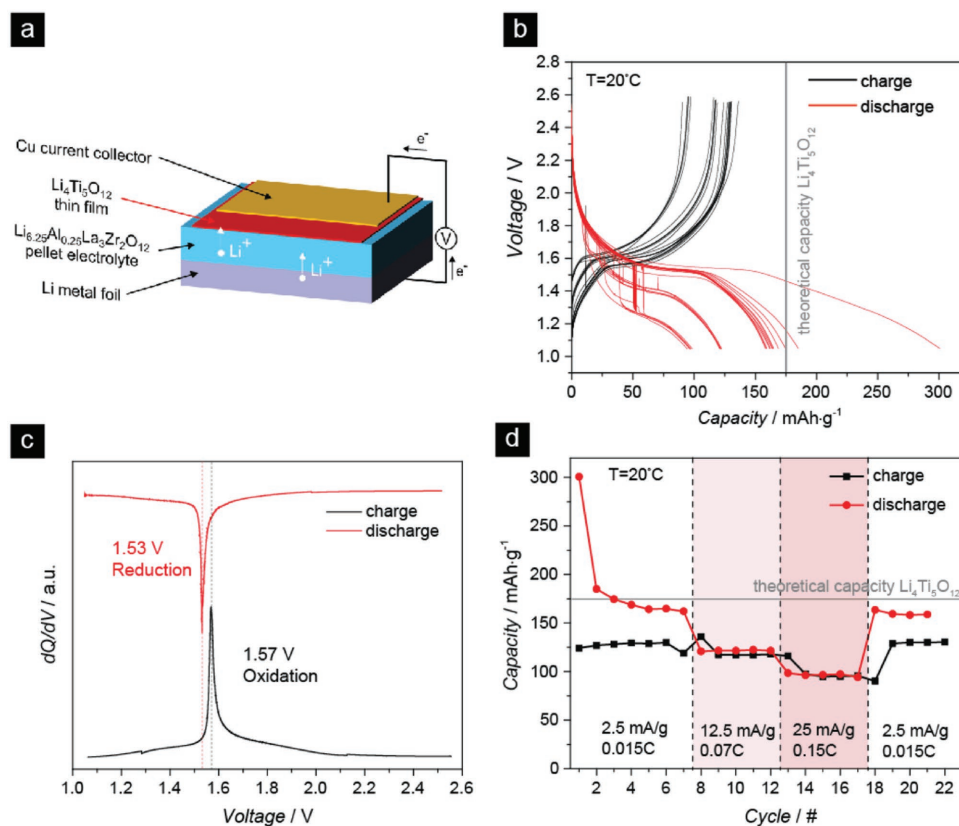


**Figure 3.** a) Sketch of a battery half-cell assembled for cycling experiments based on the system Li foil |  $\text{Li}_{6.25}\text{Al}_{0.25}\text{La}_3\text{Zr}_2\text{O}_{12}$  pellet |  $\text{Li}_4\text{Ti}_5\text{O}_{12}$  thin film | Cu current collector. Tungsten needles (black) were used to contact top and bottom electrodes. b) Charge and discharge profiles for the battery half-cell with thin film  $\text{Li}_4\text{Ti}_5\text{O}_{12}$  electrode. The typical voltage plateau of  $\text{Li}_4\text{Ti}_5\text{O}_{12}$  at around 1.5 V can be clearly observed. c)  $dQ/dV$ -plot of cycle number 3 at rate of  $2.5 \text{ mA g}^{-1}$ . d) Rate capability study of the same cell under different current rates. The discharge rate (red) was higher with respect to the charge rate (black).

film thickness reaching into cubic garnet  $\text{Li}_{6.25}\text{Al}_{0.25}\text{La}_3\text{Zr}_2\text{O}_{12}$  whose Raman modes have already been described by several authors and matching well to the ones observed here.<sup>[25,73,75,76]</sup>

We confirm that the observed spectrum shows existence of both desired structure types for the battery and near order, namely, the spinel phase for thin film of  $\text{Li}_4\text{Ti}_5\text{O}_{12}$  as well as  $\text{Li}_{6.25}\text{Al}_{0.25}\text{La}_3\text{Zr}_2\text{O}_{12}$  from the underlying electrolyte substrate after processing which is subjected in the following as half-cells for battery tests.

### 2.3. All-Solid-State Battery from Thin Film $\text{Li}_4\text{Ti}_5\text{O}_{12}$ and Cubic Garnet $\text{Li}_{6.25}\text{Al}_{0.25}\text{La}_3\text{Zr}_2\text{O}_{12}$

The successful deposition of  $\text{Li}_4\text{Ti}_5\text{O}_{12}$  phase therefore gave rise to an assembly of a battery cell: **Figure 3a** shows the schematic of the cell measured ( $\text{Li}_{6.25}\text{Al}_{0.25}\text{La}_3\text{Zr}_2\text{O}_{12}$ , with the  $\text{Li}_4\text{Ti}_5\text{O}_{12}$  thin film), including a current collector of Cu and Li metal foil as reference. Chemical comparability of the  $\text{Li}_4\text{Ti}_5\text{O}_{12}$  thin film deposited on MgO and on the garnet pellet was based on the assumption that a close phase transfer of  $\text{Li}_4\text{Ti}_5\text{O}_{12}$  is present; however, changes in the interface chemistry by nature of different substrate have to be accounted. We demonstrate the successful galvanostatic charge and discharge profiles for the assembled cell (**Figure 3b**) over 22 cycles. A discharge capacity of

$\approx 300 \text{ mAh g}^{-1}$  is obtained at the 1st discharge cycle that recovers close to the expected theoretical value of  $\approx 175 \text{ mAh g}^{-1}$  at the subsequent cycles. Note that we assign the irreversible discharge capacity obtained in the 1st cycle to potential additional oxide and hydroxide phases present at the solid electrolyte/ $\text{Li}_4\text{Ti}_5\text{O}_{12}$  interface as a result of the air exposure. In order to exclude the formation of  $\text{TiO}_2$  (anatase or rutile) impurity phases, the Raman spectra of both grown  $\text{Li}_4\text{Ti}_5\text{O}_{12}$  thin films on MgO as well as on the  $\text{Li}_{6.25}\text{Al}_{0.25}\text{La}_3\text{Zr}_2\text{O}_{12}$  pellet have been compared to powder reference spectra of  $\text{TiO}_2$  anatase as well as  $\text{TiO}_2$  rutile, as shown in **Figure S3** in the Supporting Information. Typical charge and discharge plateaus for  $\text{Li}_4\text{Ti}_5\text{O}_{12}$  can be clearly observed and the cycling is reversible for the tested cell. In **Figure 3c**, the  $dQ/dV$  plot taken from the 3rd charge/discharge cycle also corroborates our findings with oxidation and reduction peaks at 1.57 and 1.53 V, that can be clearly assigned to  $\text{Li}_4\text{Ti}_5\text{O}_{12}$ , and comparable to similar solid<sup>[44]</sup> and liquid<sup>[49]</sup> electrolyte-based batteries operating with  $\text{Li}_4\text{Ti}_5\text{O}_{12}$  slurry-cast anodes in literature. Oxidation and reduction peaks show the polarization in the system that can be quite expected in an all-solid-state cell due to interface resistance effects. The rate capability test within the first 22 cycles is shown in **Figure 3d**. The battery cell was tested with charge/discharge rates of  $2.5 \text{ mA g}^{-1}$  ( $6.3 \times 10^{-5} \text{ mA cm}^{-2}$ ),  $12.5 \text{ mA g}^{-1}$  ( $3.1 \times 10^{-4} \text{ mA cm}^{-2}$ ),  $25 \text{ mA g}^{-1}$  ( $6.3 \times 10^{-4} \text{ mA cm}^{-2}$ ), followed by  $2.5 \text{ mA g}^{-1}$  ( $6.3 \times 10^{-5} \text{ mA cm}^{-2}$ ). Due to the nature of the

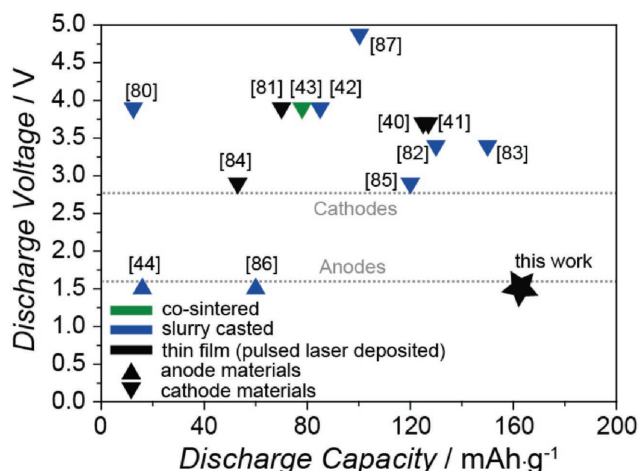


**Figure 4.** Overview on published work<sup>[40–44,80–87]</sup> on garnet LLZO-based battery assemblies in voltage versus achieved gravimetric capacity representation. Different deposition techniques are distinguished by color. Black indicating thin film electrode work, blue indicating any type of slurry deposition technique, and green standing for cosintering approaches.

low cycling speed chosen, stable operation of the cell was maintained for 29 d. Though the Coulombic efficiency is rather limited at lower rates (e.g., 2.5 mA g<sup>-1</sup>), it recovers to above ≈95% at the higher rates (e.g., 12.5 mA g<sup>-1</sup>). A discharge capacity of 97 mAh g<sup>-1</sup> is obtained at the 15th cycle even at the highest rate of 25 mA g<sup>-1</sup> that is an encouraging value considering the similar Li<sub>6.25</sub>Al<sub>0.25</sub>La<sub>3</sub>Zr<sub>2</sub>O<sub>12</sub>-based solid-state systems which are not thin film based and often operate at higher than room temperature.<sup>[44]</sup>

In summary, Li<sub>4</sub>Ti<sub>5</sub>O<sub>12</sub> thin film/Li<sub>6.25</sub>Al<sub>0.25</sub>La<sub>3</sub>Zr<sub>2</sub>O<sub>12</sub> pellet/Li batteries could successfully be used to build and cycle the first thin film-based anode/Li<sub>6.25</sub>Al<sub>0.25</sub>La<sub>3</sub>Zr<sub>2</sub>O<sub>12</sub>-system with characteristic and reproducible voltage plateau at around 1.5 V close to theoretical capacity of 175 mAh g<sup>-1</sup>. In comparison to literature work on Li-garnet all solid state batteries, one could state that the results demonstrated in this work are a step forward in the field of all-solid-state batteries based on Li<sub>6.25</sub>Al<sub>0.25</sub>La<sub>3</sub>Zr<sub>2</sub>O<sub>12</sub> solid electrolytes (see Figure 4). The previous investigations of thin film electrodes with Li<sub>6.25</sub>Al<sub>0.25</sub>La<sub>3</sub>Zr<sub>2</sub>O<sub>12</sub> solid electrolytes delivering capacities close to the theoretical values under stable cycling conditions mostly focused on cathodes (e.g., (LiCoO<sub>2</sub>) from Ohta et al.<sup>[41]</sup>). Thus, this study gives new perspective on the use of oxide-based low voltage anodes for future strategies avoiding Li-dendrite formation or safe solid state microbattery thin film assemblies based on Li-garnets.

### 3. Conclusion

In this work, we demonstrate that Li-garnet electrolytes processed as pellets and combined with Li<sub>4</sub>Ti<sub>5</sub>O<sub>12</sub> thin films can show stable cycling kinetics and reach almost close to theoretical capacity of 175 mAh g<sup>-1</sup>. We demonstrate here the stable operation at room temperature during 29 d with 90% of theoretical capacity retention at 2.5 mA g<sup>-1</sup> over 22 cycles. The results clearly indicate two implications to the all solid state battery field and technology: First, although a lot of effort was

already put in the development of suitable cathode materials for garnet electrolyte-based batteries, the conducted work positions itself as one of the first successful attempts to also implement thin film anode materials. This represents an important step forward toward the successful fabrication of full metal oxide-based batteries with Li<sub>7</sub>La<sub>3</sub>Zr<sub>2</sub>O<sub>12</sub> electrolyte compounds. It also opens up new pathways in fabrication of future batteries with various solid oxide electrode materials, as well as to form fully ceramic microbatteries possibly on chips. Second, we report by the stable cycling kinetics a high stability of the Li<sub>4</sub>Ti<sub>5</sub>O<sub>12</sub> oxide anode toward Li<sub>6.25</sub>Al<sub>0.25</sub>La<sub>3</sub>Zr<sub>2</sub>O<sub>12</sub> which is of relevance in view of current Li-dendrites forming easily for systems with metallic lithium anode solely.<sup>[60]</sup> Density functional theory calculations by the Ceder group<sup>[77]</sup> suggest that Li<sub>4</sub>Ti<sub>5</sub>O<sub>12</sub> with its voltage plateau around 1.5 V fits perfect into the stability window of the presented electrolyte and agree with the presented findings. This benchmarks the suitability of oxide-based anodes such as Li<sub>4</sub>Ti<sub>5</sub>O<sub>12</sub> as alternative to lithium for safe microbattery to large-scale storage.

### 4. Experimental Section

**Material Synthesis of the Li-Garnet Electrolyte Pellet Substrates:** Li<sub>6.25</sub>Al<sub>0.25</sub>La<sub>3</sub>Zr<sub>2</sub>O<sub>12</sub> powder was synthesized and dense pellets were prepared from it based on the methods shown by Van den Broek et al. in ref. [44]. Stable sols were obtained by dissolving stoichiometric amounts of LiNO<sub>3</sub> (99.99%, Merck), La(NO<sub>3</sub>)<sub>3</sub>(H<sub>2</sub>O)<sub>6</sub> (99.9%, Alfa Aesar), and zirconium(IV) 2,4-pentanedionate (Alfa Aesar) in a water and ethanol mixture which were fired at 600–650 °C after drying. After uniaxial as well as isostatic pressing (440 bar for 3 min) sintering took place at 1050 °C for 12 h. Sintered pellets of 11 mm in diameter were obtained and all showed >85% of theoretical density and initial thicknesses of around 1.2 mm. They were polished equally on both sides to <600 μm (see the Supporting Information for a detailed description of the polishing process).

The corresponding reference materials for Raman analysis Li<sub>4</sub>Ti<sub>5</sub>O<sub>12</sub> (>99% Aldrich) TiO<sub>2</sub> (rutile, 99.5% Aldrich) as well as TiO<sub>2</sub> (anatase, 99.7% Aldrich) were delivered from Aldrich and used as received.

**Thin Film Processing of Li<sub>4</sub>Ti<sub>5</sub>O<sub>12</sub> Anodes:** It was first turned to the processing of a suitable target for Li<sub>4</sub>Ti<sub>5</sub>O<sub>12</sub> to deposit in Pulsed Laser Deposition eventually the films. For this, dense Li<sub>4</sub>Ti<sub>5</sub>O<sub>12</sub> pellets were sintered for their use as target in PLD. In accordance, Li<sub>4</sub>Ti<sub>5</sub>O<sub>12</sub> (Sigma-Aldrich, >99% purity) and Li<sub>2</sub>O (Alfa Aesar, 99.5% purity) were used as initial precursors in the adequate amount to match a final nominal stoichiometry of Li<sub>7.1</sub>Ti<sub>5</sub>O<sub>12</sub>. A solid state route was used for the synthesis, for which the powders were first mixed under inert atmosphere inside an Ar-filled glovebox and grounded in an agate mortar and then calcined at 850 °C for 12 h. Reground powder was pressed into pellets, then uniaxially pressed followed by cold isostatic pressing (440 bar for 2 min) and sintered in an alumina-tube-furnace under constant flow of 30 sccm O<sub>2</sub>. The sintering was conducted at 1000 °C for 12 h with heating and cooling ramp rates of 5 °C min<sup>-1</sup>. With this, pellets with 82% relative densities were achieved. Pellets were then stored in an argon-filled glovebox to avoid exposure to CO<sub>2</sub> and humidity and their surface polished thoroughly prior their use as targets for pulsed laser thin film deposition.

Eventually, the fabricated targets were used to deposit thin films of Li<sub>4</sub>Ti<sub>5</sub>O<sub>12</sub> by means of pulsed laser deposition. The deposition equipment (PLD, Surface, Germany) was equipped with a KrF excimer laser of 248 nm wavelength and films were deposited at a frequency of 10 Hz with a target to substrate distance of 70 mm and background pressures of 13 mTorr O<sub>2</sub>. The temperature of the substrate was kept constant at 500 °C during thin film growth. Two different substrates were used for thin film deposition in this study: First, (001) oriented MgO

substrates (Crystec, Germany) were used for thin film structural and electrochemical analysis. Then,  $\text{Li}_4\text{Ti}_5\text{O}_{12}$  films were grown on top of the  $\text{Li}_{6.25}\text{Al}_{0.25}\text{La}_3\text{Zr}_2\text{O}_{12}$  electrolyte pellets, for building and testing all-solid-state Li-ion cells. In all of the cases, the resulting thickness of the thin film was adjusted by the number of laser shots applied, extrapolating linearly from measured growth rates by profilometry (Bruker Dektak, USA).

**Electrolyte  $\text{Li}_{6.25}\text{Al}_{0.25}\text{La}_3\text{Zr}_2\text{O}_{12}$  Pellet and Anode  $\text{Li}_4\text{Ti}_5\text{O}_{12}$  Thin Film Structural Characterization:**  $\text{Li}_{7.1}\text{Ti}_5\text{O}_{12}$  pellets as well as  $\text{Li}_{6.25}\text{Al}_{0.25}\text{La}_3\text{Zr}_2\text{O}_{12}$  electrolyte pellets were characterized by X-ray diffraction (XRD, Bruker D8, USA) with Cu K. Microstructure of the deposited thin films were investigated by scanning electron microscopy (SEM, Leo 1530, Germany). Raman spectroscopy at 10 mW power and 532 nm wavelength to ensure low required penetration depth (WiTec, Germany, spectral resolution of  $0.7\text{ cm}^{-1}$ ) was used for near order structural analysis.

**Electrochemical Characterization of Thin Films and All-Solid-State Cells:** Electrical impedance spectroscopy was performed for electrochemical analysis of the fabricated thin films. An in-plane geometry was used, with 100 nm thick electron beam evaporated platinum electrodes of lateral dimensions of  $3.25\text{ mm} \times 0.5\text{ mm}$ , separated 0.25 mm (Plassys MEB 550, France)—see inset picture in Figure 1c. An impedance measurement device (Zahner IM6, Germany) was attached to a heated Linkam stage (Linkam Scientific, UK) and the respective Nyquist data in the frequency range of 1 Hz to 1 MHz was analyzed with ZView 3.4f and OriginPro 9.1. In order to measure Arrhenius activation energies of thin films, samples were heated between 50 and 400 °C under synthetic air flow of 50 sccm. At each temperature, samples were stabilized for several minutes to assure an equilibrium was reached before any measurements took place.

Battery cells of the  $\text{Li}_{6.25}\text{Al}_{0.25}\text{La}_3\text{Zr}_2\text{O}_{12}$  pellets with  $\text{Li}_4\text{Ti}_5\text{O}_{12}$  thin films deposited on one side were then built. The complete cell was built by depositing 100 nm of copper (Plassys MEB 550, France) on top of the  $\text{Li}_4\text{Ti}_5\text{O}_{12}$  thin film working electrode for current collection and pressing a Li-metal foil on the backside of the pellet acting as the reference and counter electrode. Prior to press contacting of the Li-metal, both the pellet and the Li-foil were polished thoroughly to remove any resistive  $\text{Li}_2\text{CO}_3$  (which is prone to form on  $\text{Li}_{6.25}\text{Al}_{0.25}\text{La}_3\text{Zr}_2\text{O}_{12}$  pellets),<sup>[73]</sup> as well as traces on the surface of the Li-metal. All cell construction experiments were carried out inside an Ar-filled glovebox. In order to maintain good contact between the Li-foil and the pellet, a ceramic disc of 5 mm diameter has been used to firmly press the pellet to the Li-foil and ensure good contact. The cell geometry and design can be seen in Figure 3a. Electrical contacts were done through tungsten needle contacts placed directly on top of the Li-foil and the platinum or copper top contact, respectively.

Galvanostatic cycling was carried out inside the glovebox with a source measurement unit (Keithley 2602B, USA) with own written code (Python)<sup>[78]</sup> and took place between 1.0 and 2.6 V. Measurements were carried out at room temperature. The applied current rate for the following galvanostatic cycling was calculated with the assumption of a dense, homogeneously flat thin film of constant thickness of 80 nm. Rates between 2.5 and 25  $\text{mA g}^{-1}$  were applied. The effective area of active electrode which was broken away was kept minimal and the new geometry of the cell was measured by top view microscopy image and ImageJ was used to assess the new surface area with high accuracy.

## Supporting Information

Supporting Information is available from the Wiley Online Library or from the author.

## Acknowledgements

The authors thank the company ALSTOM for financial support and the Competence Center Energy and Mobility (CCEM) and Swisselectrics for

funding of the projects: Proposal 911 “All Solid State Li-Ion Batteries based on New Ceramic Li-Ion Electrolytes.”

## Conflict of Interest

The authors declare no conflict of interest.

## Keywords

garnets,  $\text{Li}_7\text{La}_3\text{Zr}_2\text{O}_{12}$  (LLZO), lithium titanate (LTO), solid-state batteries, thin films

Received: February 2, 2018

Revised: February 18, 2018

Published online: April 14, 2018

- [1] J.-M. Tarascon, M. Armand, *Nature* **2001**, *414*, 359.
- [2] E. Quartarone, P. Mustarelli, *Chem. Soc. Rev.* **2011**, *40*, 2525.
- [3] J. F. M. Oudenhoven, L. Baggetto, P. H. L. Notten, *Adv. Energy Mater.* **2011**, *1*, 10.
- [4] B. Y. Ahn, E. B. Duoss, M. J. Motala, X. Guo, S.-I. Park, Y. Xiong, J. Yoon, R. G. Nuzzo, J. A. Rogers, J. A. Lewis, *Science* **2009**, *323*, 1590.
- [5] N. Kwasniewski, Note7-Fiasko: Samsung senkt Gewinnerwartung, *Wirtschaft. Spieg. ONLINE*, Hamburg **2016**.
- [6] H. Esmaeilzadeh, E. Blem, R. S. Amant, K. Sankaralingam, D. Burger, in *Computer Architecture (ISCA), 2011 38th Annual International Symposium on*, IEEE, San Jose, CA, USA **2011**, pp. 365–376.
- [7] K. Sun, T.-S. Wei, B. Y. Ahn, J. Y. Seo, S. J. Dillon, J. A. Lewis, *Adv. Mater.* **2013**, *25*, 4539.
- [8] P. H. L. Notten, F. Roozeboom, R. A. H. Niessen, L. Baggetto, *Adv. Mater.* **2007**, *19*, 4564.
- [9] J. H. Pikul, H. Gang Zhang, J. Cho, P. V. Braun, W. P. King, *Nat. Commun.* **2013**, *4*, 1732.
- [10] B. J. Neudecker, N. J. Dudney, J. B. Bates, *J. Electrochem. Soc.* **2000**, *147*, 517.
- [11] M. Baba, N. Kumagai, H. Fujita, K. Ohta, K. Nishidate, S. Kornaba, B. Kaplan, H. Groult, D. Devilliers, *J. Power Sources* **2003**, *119–121*, 914.
- [12] N. Kuwata, J. Kawamura, K. Toribami, T. Hattori, N. Sata, *Electrochem. Commun.* **2004**, *6*, 417.
- [13] P. Knauth, *Solid State Ionics* **2009**, *180*, 911.
- [14] P. Hartmann, T. Leichtweiss, M. R. Busche, M. Schneider, M. Reich, J. Sann, P. Adelhelm, J. Janek, *J. Phys. Chem. C* **2013**, *117*, 21064.
- [15] H. Aono, E. Sugimoto, Y. Sadaoka, N. Imanaka, G. Adachi, *J. Electrochem. Soc.* **1989**, *136*, 590.
- [16] G. Delaizir, V. Viallet, A. Aboulaich, R. Bouchet, L. Tortet, V. Seznec, M. Morcrette, J.-M. Tarascon, P. Rozier, M. Dollé, *Adv. Funct. Mater.* **2012**, *22*, 2140.
- [17] T. Kobayashi, Y. Imade, D. Shishihara, K. Homma, M. Nagao, R. Watanabe, T. Yokoi, A. Yamada, R. Kanno, T. Tatsumi, *J. Power Sources* **2008**, *182*, 621.
- [18] Y. Deng, C. Eames, B. Fleutot, R. David, J.-N. Chotard, E. Suard, C. Masquelier, M. S. Islam, *ACS Appl. Mater. Interfaces* **2017**, *9*, 7050.
- [19] H. Y.-P. Hong, *Mater. Res. Bull.* **1978**, *13*, 117.
- [20] J. B. Bates, N. J. Dudney, G. R. Gruzalski, R. A. Zuhr, A. Choudhury, C. F. Luck, J. D. Robertson, *J. Power Sources* **1993**, *43*, 103.
- [21] V. Thangadurai, S. Narayanan, D. Pinzaru, *Chem. Soc. Rev.* **2014**, *43*, 4714.
- [22] R. Murugan, V. Thangadurai, W. Weppner, *Angew. Chem., Int. Ed.* **2007**, *46*, 7778.

- [23] J. Awaka, N. Kijima, H. Hayakawa, J. Akimoto, *J. Solid State Chem.* **2009**, *182*, 2046.
- [24] J. Awaka, A. Takashima, K. Kataoka, N. Kijima, Y. Idemoto, J. Akimoto, *Chem. Lett.* **2011**, *40*, 60.
- [25] S. Afyon, F. Krumeich, J. L. M. Rupp, *J. Mater. Chem. A* **2015**, *3*, 18636.
- [26] G. T. Hitz, E. D. Wachsman, V. Thangadurai, *J. Electrochem. Soc.* **2013**, *160*, A1248.
- [27] C. Bernuy-Lopez, W. Manalastas, J. M. Lopez del Amo, A. Aguadero, F. Aguesse, J. A. Kilner, *Chem. Mater.* **2014**, *26*, 3610.
- [28] J. Wolfenstine, J. Ratchford, E. Rangasamy, J. Sakamoto, J. L. Allen, *Mater. Chem. Phys.* **2012**, *134*, 571.
- [29] D. Rettenwander, G. Redhammer, F. Preishuber-Pflügl, L. Cheng, L. Miara, R. Wagner, A. Welzl, E. Suard, M. M. Doeff, M. Wilkening, J. Fleig, G. Amthauer, *Chem. Mater.* **2016**, *28*, 2384.
- [30] M. A. Howard, O. Clemens, K. S. Knight, P. A. Anderson, S. Hafiz, P. M. Panchmatia, P. R. Slater, *J. Mater. Chem. A* **2013**, *1*, 14013.
- [31] W. G. Zeier, S. Zhou, B. Lopez-Bermudez, K. Page, B. C. Melot, *ACS Appl. Mater. Interfaces* **2014**, *6*, 10900.
- [32] J. Wolfenstine, J. L. Allen, *J. Power Sources* **2008**, *180*, 582.
- [33] D. Rettenwander, A. Welzl, L. Cheng, J. Fleig, M. Musso, E. Suard, M. M. Doeff, G. J. Redhammer, G. Amthauer, *Inorg. Chem.* **2015**, *54*, 10440.
- [34] H. Buschmann, S. Berendts, B. Mogwitz, J. Janek, *J. Power Sources* **2012**, *206*, 236.
- [35] A. Wachter-Welzl, R. Wagner, D. Rettenwander, S. Taibl, G. Amthauer, J. Fleig, *J. Electroceramics* **2017**, *38*, 176.
- [36] L. Cheng, J. S. Park, H. Hou, V. Zorba, G. Chen, T. Richardson, J. Cabana, R. Russo, M. Doeff, *J. Mater. Chem. A* **2014**, *2*, 172.
- [37] S. Afyon, F. Krumeich, C. Mensing, A. Borgschulte, R. Nesper, *Sci. Rep.* **2014**, *4*, 7113.
- [38] X. Ji, K. T. Lee, L. F. Nazar, *Nat. Mater.* **2009**, *8*, 500.
- [39] C. Hänsel, S. Afyon, J. L. M. Rupp, *Nanoscale* **2016**, *8*, 18412.
- [40] S. Ohta, T. Kobayashi, T. Asaoka, *J. Power Sources* **2011**, *196*, 3342.
- [41] S. Ohta, T. Kobayashi, J. Seki, T. Asaoka, *J. Power Sources* **2012**, *202*, 332.
- [42] S. Ohta, S. Komagata, J. Seki, T. Saeki, S. Morishita, T. Asaoka, *J. Power Sources* **2013**, *238*, 53.
- [43] S. Ohta, J. Seki, Y. Yagi, Y. Kihira, T. Tani, T. Asaoka, *J. Power Sources* **2014**, *265*, 40.
- [44] J. Van den Broek, S. Afyon, J. L. M. Rupp, *Adv. Energy Mater.* **2016**, *6*, 1600736.
- [45] Y. Jin, P. J. McGinn, *J. Power Sources* **2011**, *196*, 8683.
- [46] R. K. Gover, J. R. Tolchard, H. Tukamoto, T. Murai, J. T. Irvine, *J. Electrochem. Soc.* **1999**, *146*, 4348.
- [47] J. B. Goodenough, Y. Kim, *Chem. Mater.* **2010**, *22*, 587.
- [48] G. G. Amatucci, F. Badway, A. Du Pasquier, T. Zheng, *J. Electrochem. Soc.* **2001**, *148*, A930.
- [49] K. M. Colbow, J. R. Dahn, R. R. Haering, *J. Power Sources* **1989**, *26*, 397.
- [50] S. Scharner, *Untersuchungen zur Struktur, Elektrochemie und Farbe von substituierten Lithiumtitanaten für mögliche Anwendungen in der Elektrochromie*, Berichte aus der Chemie, Als Ms. gedr., Shaker, Aachen **1998**.
- [51] A. Kumatani, S. Shiraki, Y. Takagi, T. Suzuki, T. Ohsawa, X. Gao, Y. Ikuhara, T. Hitosugi, *Jpn. J. Appl. Phys.* **2014**, *53*, 058001.
- [52] M. R. Mohammadi, D. J. Fray, *J. Sol-Gel Sci. Technol.* **2010**, *55*, 19.
- [53] J. Deng, Z. Lu, I. Belharouak, K. Amine, C. Y. Chung, *J. Power Sources* **2009**, *193*, 816.
- [54] A. Kumatani, T. Ohsawa, R. Shimizu, Y. Takagi, S. Shiraki, T. Hitosugi, *Appl. Phys. Lett.* **2012**, *101*, 123103.
- [55] D. M. Packwood, S. Shiraki, T. Hitosugi, *Phys. Rev. Lett.* **2013**, *111*, 036101.
- [56] S. Ganapathy, M. Wagemaker, *ACS Nano* **2012**, *6*, 8702.
- [57] M. Wagemaker, F. M. Mulder, *Acc. Chem. Res.* **2013**, *46*, 1206.
- [58] Y. Shi, A. H. Bork, S. Schweiger, J. L. M. Rupp, *Nat. Mater.* **2015**, *14*, 721.
- [59] S. Schweiger, R. Pfenninger, W. J. Bowman, U. Aschauer, J. L. M. Rupp, *Adv. Mater.* **2017**, *29*, 1605049.
- [60] F. Aguesse, W. Manalastas, L. Buannic, J. M. Lopez del Amo, G. Singh, A. Llordés, J. Kilner, *ACS Appl. Mater. Interfaces* **2017**, *9*, 3808.
- [61] E. Ferg, R. J. Gummow, A. De Kock, M. M. Thackeray, *J. Electrochem. Soc.* **1994**, *141*, L147.
- [62] T. Ohzuku, A. Ueda, N. Yamamoto, *J. Electrochem. Soc.* **1995**, *142*, 1431.
- [63] D. C. Johnston, *J. Low Temp. Phys.* **1976**, *25*, 145.
- [64] K. Mukai, Y. Kato, H. Nakano, *J. Phys. Chem. C* **2014**, *118*, 2992.
- [65] T.-F. Yi, Y. Xie, Y.-R. Zhu, R.-S. Zhu, H. Shen, *J. Power Sources* **2013**, *222*, 448.
- [66] I. A. Leonidov, O. N. Leonidova, L. A. Perelyaeva, R. F. Samigullina, S. A. Kovyazina, M. V. Patrakeeve, *Phys. Solid State* **2003**, *45*, 2183.
- [67] K. T. Fehr, M. Holzapfel, A. Laumann, E. Schmidbauer, *Solid State Ionics* **2010**, *181*, 1111.
- [68] M. Wilkening, R. Amade, W. Iwaniak, P. Heitjans, *Phys. Chem. Chem. Phys.* **2007**, *9*, 1239.
- [69] H. Lindström, S. Södergren, A. Solbrand, H. Rensmo, J. Hjelm, A. Hagfeldt, S.-E. Lindquist, *J. Phys. Chem. B* **1997**, *101*, 7710.
- [70] I. Kosacki, C. M. Rouleau, P. F. Becher, J. Bentley, D. H. Lowndes, *Solid State Ionics* **2005**, *176*, 1319.
- [71] M. Rawlence, I. Garbayo, S. Buecheler, J. L. M. Rupp, *Nanoscale* **2016**, *8*, 14746.
- [72] M. V. F. Schlupp, M. Prestat, J. Martynczuk, J. L. M. Rupp, A. Bieberle-Hütter, L. J. Gauckler, *J. Power Sources* **2012**, *202*, 47.
- [73] G. Larraz, A. Orera, M. L. Sanjuán, *J. Mater. Chem. A* **2013**, *1*, 11419.
- [74] L. Cheng, C. H. Wu, A. Jarry, W. Chen, Y. Ye, J. Zhu, R. Kostecki, K. Persson, J. Guo, M. Salmeron, G. Chen, M. Doeff, *ACS Appl. Mater. Interfaces* **2015**, *7*, 17649.
- [75] T. Thompson, J. Wolfenstine, J. L. Allen, M. Johannes, A. Huq, I. N. David, J. Sakamoto, *J. Mater. Chem. A* **2014**, *2*, 13431.
- [76] F. Tietz, T. Wegener, M. T. Gerhards, M. Giarola, G. Mariotto, *Solid State Ionics* **2013**, *230*, 77.
- [77] L. J. Miara, W. D. Richards, Y. E. Wang, G. Ceder, *Chem. Mater.* **2015**, *27*, 4040.
- [78] Unified Measurement Software UMS, ETH Zürich, <https://doi.org/10.3929/ethz-b-000247100> (accessed: December 2017).
- [79] S. Hayashi, H. Hatano, *J. Ceram. Soc. Jpn.* **1994**, *102*, 378.
- [80] M. Kotobuki, K. Kanamura, Y. Sato, T. Yoshida, *J. Power Sources* **2011**, *196*, 7750.
- [81] T. Kato, T. Hamaoka, K. Yamamoto, T. Hirayama, F. Sagane, M. Motoyama, Y. Iriyama, *J. Power Sources* **2014**, *260*, 292.
- [82] K. (Kelvin) Fu, Y. Gong, B. Liu, Y. Zhu, S. Xu, Y. Yao, W. Luo, C. Wang, S. D. Lacey, J. Dai, Y. Chen, Y. Mo, E. Wachsman, L. Hu, *Sci. Adv.* **2017**, *3*, e1601659.
- [83] F. Du, N. Zhao, Y. Li, C. Chen, Z. Liu, X. Guo, *J. Power Sources* **2015**, *300*, 24.
- [84] Y. Jin, P. J. McGinn, *J. Power Sources* **2013**, *239*, 326.
- [85] Y. Jin, P. J. McGinn, *Electrochim. Acta* **2013**, *89*, 407.
- [86] J. van den Broek, J. L. M. Rupp, S. Afyon, *J. Electroceramics* **2017**, *38*, 182.
- [87] X. Han, Y. Gong, K. (Kelvin) Fu, X. He, G. T. Hitz, J. Dai, A. Pearse, B. Liu, H. Wang, G. Rubloff, Y. Mo, V. Thangadurai, E. D. Wachsman, L. Hu, *Nat. Mater.* **2017**, *16*, 572.